Numerical simulation of a hybrid trapped field magnet lens (HTFML) magnetized by pulsed fields

Numerical simulation of a hybrid trapped field magnet lens (HTFML) magnetized by pulsed fields

Motoki Shinden[1], Sora Namba[1], Tatsuya Hirano[1], Hiroyuki Fujishiro[1], Tomoyuki Naito[1] and Mark D Ainslie[2]

[1] Department of Physical Science and Materials Engineering, Faculty of Science and Engineering, Iwate University, 4-3-5 Ueda, Morioka 020-8551, Japan
[2] Department of Engineering, University of Cambridge, Trumpington Street, Cambridge CB2 1PZ, United Kingdom

Email : s0416027@iwate-u.ac.jp

Abstract. The hybrid trapped field magnet lens (HTFML) is a promising device that is able to concentrate a magnetic field higher than an applied background field continuously, even after removing a background field, which was conceptually proposed by the authors in 2018. We have numerically investigated the HTFML performance, consisting of a REBaCuO cylindrical magnetic lens and REBaCuO trapped field magnet (TFM) cylinder, magnetized by pulsed fields. Single magnetic pulses were applied ranging from B_{app} = 1.5 T to 5.0 T at the operating temperature of T_s = 30, 40 and 50 K, and the performance was compared with that of the single REBaCuO TFM cylinder. The HTFML effect was clearly confirmed for the lower B_{app} values. However, for the higher B_{app} values, the trapped field in the magnetic lens bore was nearly equal to or slightly lower than that for the single TFM cylinder because of a weakened lens effect due to magnetic flux penetration into the lens. A temperature rise in the REBaCuO magnetic lens and TFM cylinder was also observed. These results strongly suggest that lowering the temperature of the REBaCuO magnetic lens could enhance the HTFML effect even for higher B_{app}.

1. Introduction

Bulk superconductors can be used as trapped field magnets (TFMs), because they can trap a higher magnetic field by a strong 'vortex pinning effect,' which is proportional to the critical current density, $J_c(B, T)$, and the diameter of the bulk. In particular, melt-processed single-domain REBaCuO superconducting bulks (where RE is a rare earth element or Y) are a possible candidate for strong TFMs, because their J_c significantly improves by lowering the temperature. Trapped fields over 17 T below 30 K have been achieved using YBaCuO and GdBaCuO bulks by field-cooled magnetization (FCM) to date [1 - 3]. Bulk TFMs magnetized by FCM can trap a magnetic field nearly the same or slightly lower than the applied field, B_{app}. However, such high applied fields are only available from specialized, expensive superconducting magnets in a limited number of facilities worldwide. For this reason, such high-strength TFMs magnetized by FCM are generally not practical for applications, although the technique is useful for characterizing a bulk's maximum trapped field capability. Pulsed-field magnetization (PFM) is the most practical method to magnetize superconducting bulks because it is a faster magnetizing process than FCM (on the order of milliseconds) and is an inexpensive and mobile experimental setup using a copper pulsed magnet. However, the trapped field by PFM is much lower

than that by FCM because of a larger temperature rise resulting from the rapid and dynamical motion of the magnetic flux in the bulk during its magnetizing process [4 - 6]. The maximum trapped field achieved by PFM to date is 5.2 T at 29 K [7], which is significantly lower than that achieved by FCM; 17 T.

A 'magnetic lens' using a cone-shaped superconducting bulk pair has also been investigated, in which the magnetic flux is concentrated in its bore, exploiting the 'diamagnetic shielding effect' of the superconducting material. The available magnetic field is higher than the applied field generated by the external magnetizing coil [8 - 10]. A concentrated magnetic field of B_c = 12.42 T was achieved at 20 K for a background field of 8 T by using a cone-shaped GdBaCuO bulk magnetic lens [9] and B_c = 30.4 T at 4.2 K was achieved for a background field of 28.3 T [10].

We proposed a new concept of the hybrid trapped field magnet lens (HTFML) in 2018, which combines an outer bulk TFM cylinder with an inner bulk magnetic lens [11]. In the HTFML, the TFM cylinder traps and provides a static magnetic field exploiting the 'vortex pinning effect' and the inner magnetic lens concentrates the magnetic field in its bore exploiting the 'diamagnetic shielding effect'. The magnetic field generated in the HTFML bore is higher than that in the TFM cylinder itself. Using an MgB_2 bulk cylinder and GdBaCuO bulk lens, the HTFML was predicted numerically to generate a concentrated magnetic field of B_c = 4.73 T with a background magnetizing field of B_{app} = 3 T. With the HTFML consisting of a GdBaCuO bulk cylinder and GdBaCuO bulk lens, a significantly higher B_c = 13.49 T was predicted for a higher B_{app} = 10 T. Recently, we have experimentally confirmed the HTFML effect using a setup with an MgB_2 bulk cylinder and GdBaCuO bulk lens, and B_c = 3.65 T was achieved for B_{app} = 2.0 T at 20 K [12]. If the HTFML concept can be realized and the trapped field is enhanced using PFM, the practical applications of such a configuration of superconducting bulks could be expanded widely.

In the present study, we have carried out numerical simulations of the PFM of an HTFML consisting of an outer REBaCuO TFM cylinder and inner REBaCuO magnetic lens. The possibility of the magnetic field amplification by the HTFML using PFM is investigated.

2. Numerical simulation framework

A three-dimensional (3D) numerical model was constructed based on our experimental setup for PFM [13], and numerical simulations were performed using the finite element method (FEM). The commercial software package, Photo-Eddy (Photon Ltd, Japan), combined with Photo-Thermo (Photon Ltd, Japan), was adapted for the analyses. Figure 1(a) shows the cross-sectional view of the numerical model used in the simulation. The REBaCuO cylindrical magnetic lens (10 mm in inner diameter (ID), 30 mm in outer diameter (OD) and 7.5 mm in height (H)) and the REBaCuO TFM cylinder (ID = 36 mm, OD = 60 mm, H = 20 mm) are placed on the cold stage, which are aligned along their central lines. A stainless steel (SS) ring 6.25 mm in H is set below the magnetic lens to align with the center of the TFM cylinder. The bottom surface of both the SS ring and TFM cylinder are thermally connected to the cold stage of the refrigerator by a thin indium sheet and cooled to operating temperatures of T_s = 30, 40 and 50 K. The HTFML is magnetized by single pulsed magnetic fields ranging from B_{app} = 1.5 T to 5.0 T with a rise time of 13 ms and a duration of 200 ms using an outer solenoid magnetizing coil (ID = 100 mm, OD = 120 mm, H = 50 mm).

Figure 1(b) shows the top view of the magnetic lens and TFM cylinder. In the cylindrical magnetic lens, two slits of 10° wide are assumed, which are the same as those in the cone-shaped magnetic lens investigated in our previous works [11, 12]. The trapped field, B_T, for the single TFM cylinder and the concentrated field, B_c, for the HTFML along the z-direction are calculated in the inner bore (r = z = 0 mm). The electromagnetic and thermal behaviour during PFM are described by the fundamental equations shown elsewhere [14 - 16]. The power-n law (n = 20) was used to describe the nonlinear E–J characteristic of the REBaCuO superconducting bulks as

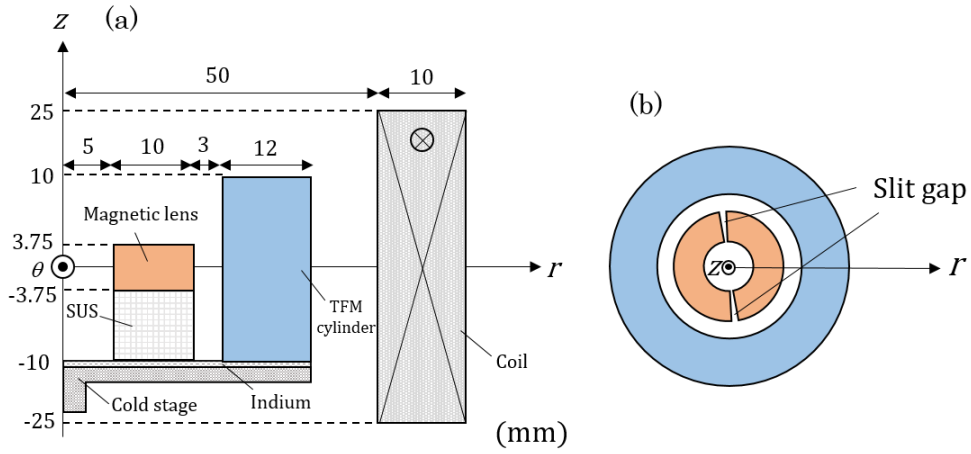

Figure 1. (a) Cross-sectional view and (b) top view of the HTFML model used in the numerical simulations.

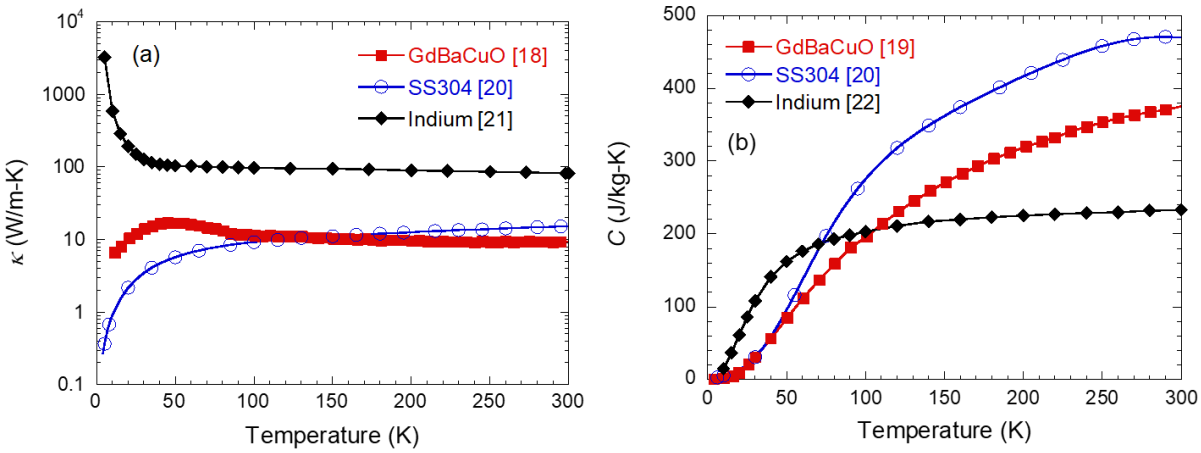

Figure 2. Temperature dependence of (a) thermal conductivity, κ, and (b) specific heat, C, of GdBaCuO, SS304 and indium assumed in the simulation.

$$E = E_c \left(\frac{J}{J_c}\right)^n, \tag{1}$$

where J_c is the critical current density of the bulks and E_c (= 10^{-4} V/m) is the characteristic electric field. For the REBaCuO bulks used in the numerical simulation, the magnetic field- and temperature-dependent critical current density, $J_c(B, T)$, proposed by Kim *et al.* [17] was adopted using the following equation,

$$J_c = \alpha \left\{1 - \left(\frac{T}{T_c}\right)^2\right\}^{\frac{3}{2}} \frac{B_0}{|B| + B_0}, \tag{2}$$

where T_c is the critical temperature (= 92 K) of the REBaCuO superconductor, B_0 = 1.3 T is a constant and α = 3.45 × 10^9 A/m^2 is the extrapolated J_c value at T = 0 K and B = 0 T. The REBaCuO bulks are assumed to be isotropic and homogenous for simplicity. The temperature dependence of the thermal

properties (thermal conductivity and specific heat) of the materials (REBaCuO bulk, SS and indium) used in the simulation are from references [18 - 22], as shown in Fig. 2.

3. Results and discussion

3.1. *Electromagnetic and thermal properties of HTFML magnetized by pulsed fields*

Figure 3(a) shows the time dependence of trapped field, $B_T(t)$, in the inner bore ($r = z = 0$ mm) for the single TFM cylinder magnetized by pulsed fields of B_{app} = 3.0 T to 4.5 T at T_s = 40 K. The time dependence of the normalized background field, $B_{ex}(t)/B_{app}$, is also shown on the right vertical axis. For B_{app} < 3.5 T, $B_T(t)$ took a maximum value and then reached its final value at t = 7 s with a slight decay. On the other hand, for B_{app} > 4 T, a large decay of B_T during the descending phase of the pulse ($t \geq$ 13 ms) can be seen, and the $B_T(t = 7\ s)$ value for B_{app} = 4.5 T was in fact lower than that for B_{app} = 4.0 T. These results come from the large temperature rise due to the rapid flux movement and the decrease in $J_c(B, T)$ of the bulks related to the higher applied field.

Figure 3(b) shows similar numerical results for the HTFML magnetized by pulsed fields of B_{app} = 3.0 T to 4.5 T at T_s = 40 K. Similar to the magnetization of the single TFM, for B_{app} < 3.5 T, the concentrated magnetic field, $B_c(t)$, took a maximum value and then reached its final value at t = 7 s with a small decay. However, the $B_c(t = 7\ s)$ value was higher than the $B_T(t = 7\ s)$ for the single TFM; the $B_c(t = 7\ s)$ values for B_{app} = 3.0 T and 3.5 T were 0.93 T and 1.61 T, respectively, which were higher than $B_T(t = 7\ s)$ = 0.55 T and 1.35 T, respectively, for the single TFM. These results suggest that the HTFML effect can be achieved by PFM for lower B_{app}. However, for B_{app} > 4.0 T, $B_c(t)$ took a maximum, which was higher than $B_T(t)$ for the single TFM, but also suffered a larger decay of $B_c(t)$ than $B_T(t)$ during descending phase of the pulse. The $B_c(t = 7\ s)$ value was 1.75 T for B_{app} = 4.0 T, which was nearly the same as $B_T(t = 7\ s)$ for the single TFM. In addition, for B_{app} = 4.5 T, the $B_c(t = 7\ s)$ value was 1.48 T, which was smaller than $B_T(t = 7\ s)$ = 1.72 T for the single TFM. The inset of Fig. 3(b) shows the magnitude of the flux flow, $B_{flow} = B_T^{max} - B_T(t = 7s)$ (or $B_c^{max} - B_c(t = 7s)$), as a function of B_{app} at 40 K. The B_{flow} value increased with the increase in B_{app} for each case. The B_{flow} value for the HTFML was higher than that for the single TFM.

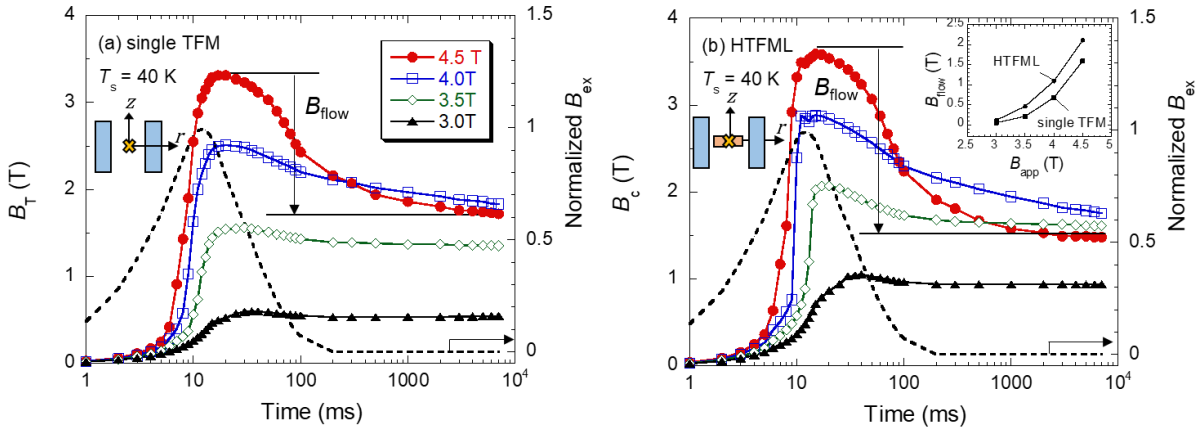

Figure 3. Time dependence of the magnetic field, (a) $B_T(t)$ for the single TFM cylinder and (b) $B_c(t)$ for the HTFML in the inner bore ($r = z = 0$ mm) at 40 K for applied fields of B_{app} = 3.0 to 4.5 T. The normalized background field (dotted curve), B_{ex}, is also shown on the right vertical axis. The applied field, B_{app}, dependence of the flux flow, B_{flow}, is shown in the inset of (b).

Figure 4 shows the time dependence of the temperature rise, ΔT, in the TFM cylinder and the magnetic lens in the same HTFML device for B_{app} = 3.0 T and 4.5 T at T_s = 40 K. The temperature was calculated at the outer edge of the TFM cylinder surface (r = 30 mm, z = 10 mm) and the inner edge of

the magnetic lens surface (r =5.0 mm, z = 3.75 mm), both of which are the locations of the highest temperature rise, being most exposed to the magnetic field. The ΔT value in the TFM cylinder increases with the increase in B_{app}, and the $\Delta T(t)$ profiles have a two-step rise which is closely related to the rate of flux movement for the ascending and descending phases of the pulsed field, as indicated in previous research [19, 23]. The temperature rise takes a maximum at around t = 1 s, which was 6 K (T_{max} = 46 K) for B_{app} = 3.0 T and 22 K (T_{max} = 62 K) for B_{app} = 4.5 T. The large temperature rise leads to the degradation of the superconducting properties and causes noticeable flux flow, as shown in Fig. 3. In contrast, for the magnetic lens, the temperature hardly increased for B_{app} = 3.0 T, for which the performance of the magnetic lens was affected minimally by the temperature rise. However, for B_{app} = 4.5 T, the temperature of the magnetic lens increases with increasing time and the maximum ΔT was 6 K, which reduces the J_c of the magnetic lens. It should be noted that the temperature rise of the magnetic lens was delayed compared to the TFM cylinder because of the magnetic shielding effect of the outer TFM cylinder.

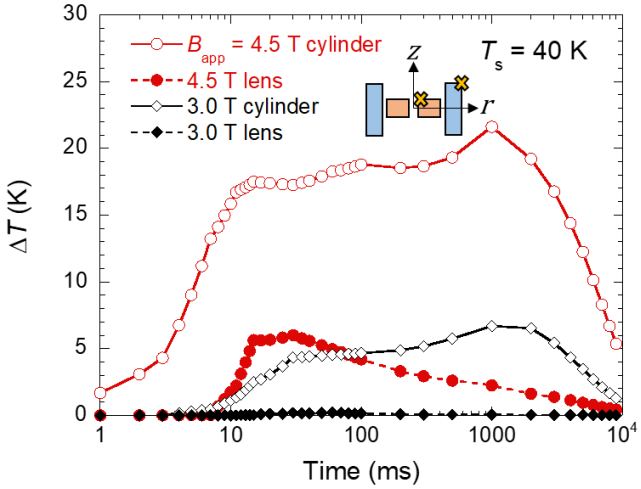

Figure 4. Temperature rise, ΔT, in the TFM cylinder and magnetic lens in the HTFML as a function of time for B_{app} = 3.0 T and 4.5 T at T_s = 40 K. The temperature was calculated at the outer edge of the TFM cylinder (r = 30 mm, z = 10 mm) and the inner edge of magnetic lens (r = 5.0 mm, z = 3.75 mm).

Figures 5(a) and 5(b), respectively, show the time dependence of the magnetic field profiles of the single TFM and HTFML for B_{app} = 3.0 T at 40 K during the descending phase of the applied pulse ($t \geq$ 13 ms). In Fig. 5(a), the magnetic field was shielded by the TFM cylinder but slightly penetrated into the cylinder bore at t = 13 ms, which was as small as 0.1 T. The trapped field within the bore slightly increased with increasing time. A flat trapped field distribution with a maximum value of only 0.3 T was observed inside the bore in the case of the single TFM. Therefore, the applied field of B_{app} = 3.0 T was not enough to fully magnetize the TFM cylinder. On the other hand, in the case of the HTFML, as shown in Fig. 5(b), the magnetic field which penetrated into the cylinder bore and passed through the slit of the magnetic lens was concentrated in the lens bore with time. Consequently, a concentrated field of about 1.0 T was achieved at t = 7 s. The magnetic field did not penetrate into the magnetic lens region (5 mm $\leq r \leq$ 15 mm and −15 mm $\leq r \leq$ −5 mm), which implies that a high $J_c(B, T)$ for the magnetic lens could be maintained against the magnetic field in the cylinder bore. As a result, the concentration and amplification of the trapped field was realized for B_{app} = 3.0 T.

Figures 5(c) and 5(d), respectively, show similar profiles of the magnetic field for the single TFM and HTFML for B_{app} = 4.5 T. In the case of the single TFM, the magnetic field penetrated significantly more into the cylinder bore at t = 13 ms, which was as large as 3.2 T. The magnetic field then decreased with increasing time, and finally reached 1.7 T at t = 7 s. For the HTFML, as shown in Fig. 5(d), the magnetic field penetrated into the lens bore at t = 13 ms, which was about 3.5 T and slightly higher than

that for the single TFM. The magnetic field in the lens bore decreased with increasing time due to the large flux flow and the final $B_c(t = 7\ \mathrm{s})$ value was 1.48 T, lower than the $B_T(t = 7\ \mathrm{s})$ value for the single TFM. It should be noted that the magnetic flux penetrated and was trapped in the magnetic lens region, which leads to the decrease in J_c in the magnetic lens due to the increase in both temperature and magnetic field. This magnetic field trapped in the magnetic lens part generates an opposing magnetic field along the −*z*-direction in the lens bore [12]. As a result, the final B_c value at $t = 7$ s decreased, compared to the trapped field for the single TFM.

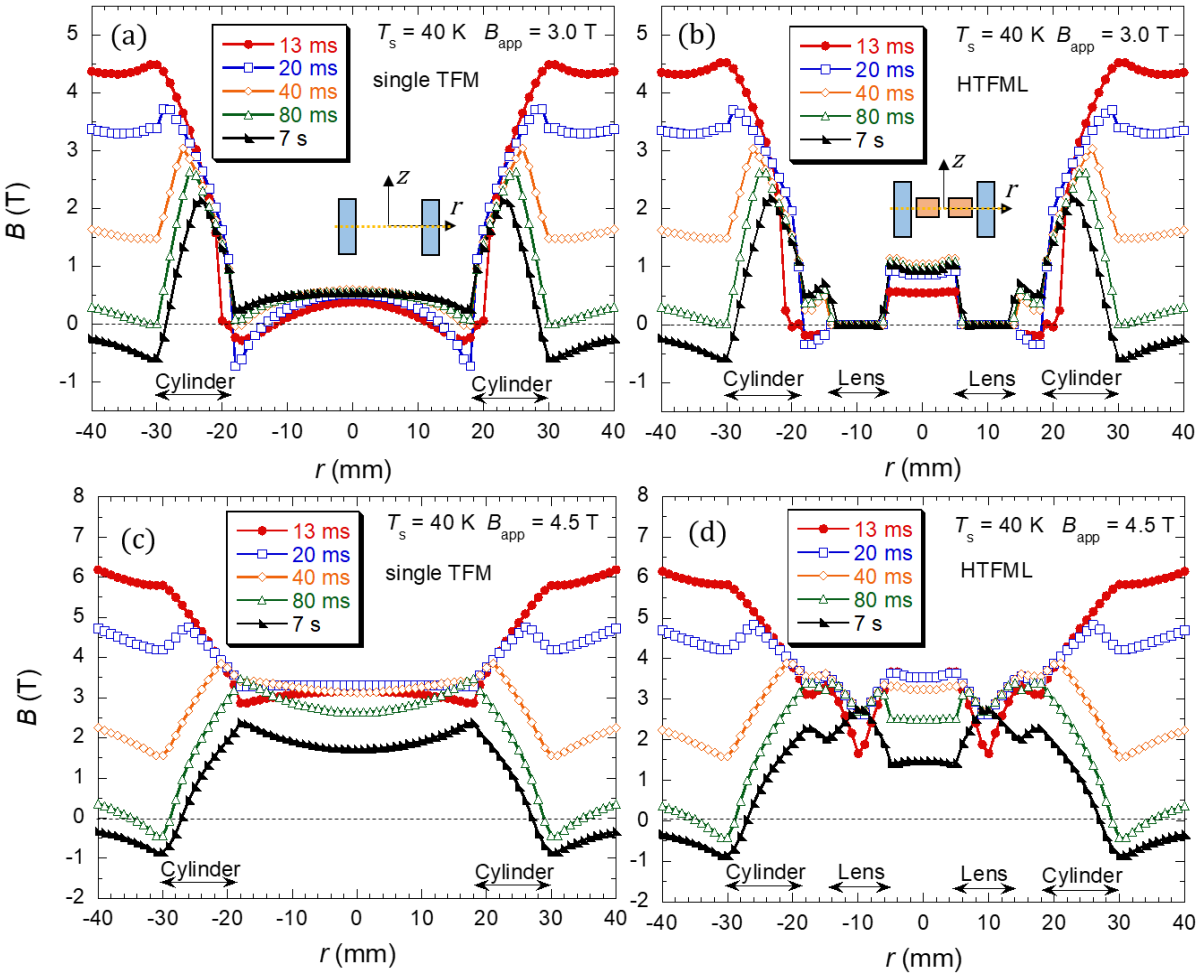

Figure 5. Time dependence of the magnetic field profiles of (a) single TFM cylinder and (b) HTFML along the *r*-direction ($z = 0$ mm) for $B_{app} = 3.0$ T at $T_s = 40$ K. Similar profiles are also shown for (c) single TFM cylinder and (d) HTFML for $B_{app} = 4.5$ T at $T_s = 40$ K.

3.2. Temperature dependence of final trapped field and temperature rise of HTFML.

Figure 6(a) shows the applied field dependence of the concentrated field, $B_c(t = 7\ \mathrm{s})$, and trapped field, $B_T(t = 7\ \mathrm{s})$, at $T_s = 30$, 40 and 50 K. The applied field, B_{app}, at which the magnetic flux penetrated into the TFM cylinder bore and the trapped field took a maximum, shifted to a higher field for lower T_s because the magnetic shielding effect of the TFM cylinder increases with increasing J_c. Thus, a higher applied field was required for the full penetration of the magnetic flux into the inner bore. The HTFML effect can be confirmed for lower applied fields at each T_s. For example, in the case of $T_s = 50$ K and $B_{app} = 2.5$ T, the concentrated field $B_c(t = 7\ \mathrm{s}) = 0.63$ T was 1.8 times higher than the trapped field $B_T(t = 7\ \mathrm{s}) = 0.35$ T, and at $T_s = 30$ K and $B_{app} = 3.5$ T, $B_c(t = 7\ \mathrm{s}) = 1.35$ T was 1.35 times higher than $B_T(t =$

7 s) = 1.0 T. However, it should be noted that for the higher applied fields, the maximum of the final concentrated field, $B_c(t = 7\ s)$, for the HTFML could not exceed the maximum trapped field, $B_T(t = 7\ s)$, for the single TFM at each T_s.

Figure 6 (b) shows the applied field dependence of the maximum temperature rise, ΔT_{max}, in the TFM cylinder and the magnetic lens in the same HTFML device at each operating temperature, T_s. The temperature was calculated at the outer edge of the TFM cylinder surface (r = 30 mm, z = 10 mm) and the inner edge of the magnetic lens surface (r = 5.0 mm, z = 3.75 mm). At each T_s, ΔT_{max} in each part increases with increasing B_{app} due to the dynamic flux movement. ΔT_{max} increases for lower T_s, and ΔT_{max} in the TFM cylinder was twice or three times larger than that in the magnetic lens. Since the specific heat of the bulks decreases with decreasing temperature, as shown in Fig. 2(b), the increase in ΔT_{max} is reasonable for a lower operating temperature. In the magnetic lens, the small temperature rise implies that a large concentration of magnetic field can be expected if only the magnetic lens part is cooled further. For example, if the temperature of the TFM cylinder is 40 K and the magnetic lens is cooled to 20 K, the $J_c(B, T)$ characteristics of the magnetic lens are improved and the HTFML effect for higher applied fields can be expected. In addition, a modified multi-pulse technique with step-wise cooling (M-MPSC) may be an effective method to enhance the HTFML effect [24, 25]. Using this method, the performance of the both TFM cylinder and magnetic lens could be improved.

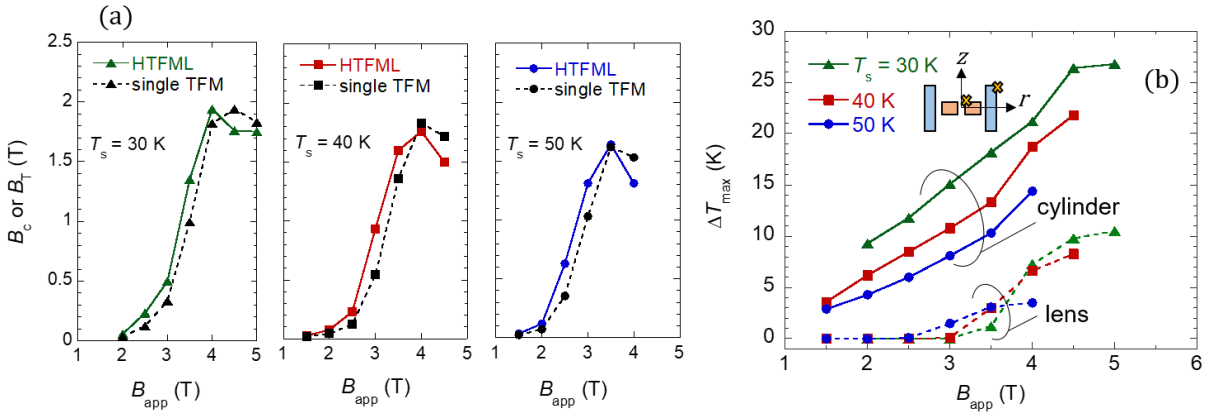

Figure 6. (a) Applied field, B_{app}, dependence of the final concentrated field, $B_c(t = 7\ s)$, for the HTFML (solid line), and the final trapped field, $B_T(t = 7\ s)$, for the single TFM cylinder (dotted line) at T_s = 30, 40 and 50 K. (b) B_{app}-dependence of the maximum temperature rise, ΔT_{max}, in the TFM cylinder and the magnetic lens at T_s = 30, 40 and 50 K.

4. Conclusion

We have numerically investigated the performance of the hybrid trapped field magnet lens (HTFML) magnetized by pulsed fields, assuming a REBaCuO cylindrical magnetic lens and REBaCuO TFM cylinder. The important results and conclusions in this study are summarized as follows.

(1) The HTFML effect was confirmed clearly for lower applied fields, B_{app}, compared with the trapped field for the single TFM cylinder under identical conditions for B_{app} and operating temperature, T_s.
(2) For higher B_{app}, the concentrated field for the HTFML was nearly equal to or slightly lower than the trapped field for the single TFM cylinder because of magnetic flux penetration and trapping in the magnetic lens.
(3) To enhance the HTFML effect for higher B_{app}, lowering the temperature of the magnetic lens with respect to the TFM cylinder is a possible solution because the $J_c(B, T)$ characteristics of the magnetic lens would be improved, and the shielding effect will be enhanced further.

Acknowledgments
This research is supported by Adaptable and Seamless Technology transfer Program through Target-driven R&D (A-STEP) from Japan Science and Technology Agency (JST), Grant No. VP30218088419 and by JSPS KAKENHI Grant No.19K05240. M D Ainslie would like to acknowledge financial support from an Engineering and Physical Sciences Research Council (EPSRC) Early Career Fellowship, EP/P020313/1. All data are provided in full in the results section of this paper.

References

[1] Tomita M and Murakami M 2003 *Nature* **421** 517–20
[2] Durrell J H *et al.* 2014 *Supercond. Sci. Technol*. **27** 082001
[3] Huang K Y *et al*. 2020 *Supercond. Sci Technol*. **33** 02LT01
[4] Ainslie M D *et al*. 2014 *Supercond. Sci. Technol.* **27** 065008
[5] Hirano T *et al*. 2019 *IEEE Trans. Appl. Supercond*. **29** 6801705
[6] Fujishiro H, Yokoyama K, Oka T and Noto K 2004 *Supercond. Sci. Technol.* **17** 51–57
[7] Fujishiro H, Tateiwa T, Fujiwara A, Oka T and Hayashi H 2006 *Physica C* **445–448** 334–8
[8] Kiyoshi T, Choi S, Matsumoto S, Asano T and Uglietti D 2009 *IEEE Trans. Appl. Supercond*. **19** 2174–7
[9] Zhang Z Y, Matsumoto S, Teranishi R and Kiyoshi T 2012 *Supercond. Sci. Technol*. **25** 115012
[10] Choi S, Yoon J-H, Lee B-S, Won M-S, Ok J-W, Zhang Z-, Kiyoshi T, Matsumoto S and Lee S-H 2012 *J. Appl. Phys.* **111** 07E728
[11] Takahashi K, Fujishiro H and Ainslie M D 2018 *Supercond. Sci. Technol.* **31** 044005
[12] Namba S, Fujishiro H, Naito T, Mark D Ainslie and Takahashi K 2019 *Supercond. Sci. Technol*. **32** 12LT03
[13] Hirano T *et al*. *IEEE Trans. Appl. Supercond*. 2019 **29** 8000705
[14] Fujishiro H, Itoh Y, Yanagi Y and Nakamura T 2015 *Supercond. Sci. Technol.* **28** 095018
[15] Ainslie M D and Fujishiro H 2015 *Supercond. Sci. Technol.* **28** 053002
[16] Fujishiro H, Naito T, Yanagi Y, Itoh Y and Nakamura T 2019 *Supercond. Sci. Technol*. **32** 065001
[17] Kim Y B, Hempstead C F and Strnad A R 1965 *Phys. Rev.* **139** A1163–72
[18] Fujishiro H, Katagiri K, Murakami A, Yoshino Y, Noto K 2005 *Physica C* **426-431** 699-704
[19] Ainslie M D *et al*. 2016 *Supercond. Sci. Technol.* **29** 074003
[20] Marquardt E, Le J and Radebaugh R 2002 *Cryocoolers* **11**, 681–687
[21] Ho C Y, Powell R W, and Liley P E 1972 *J Phys. Chem. Ref. Data*, **1(2)** , 279–421
[22] Clusius K, Schachinger L and Angew Z 1952 *Physik* **4** 442
[23] Ainslie M D *et al*. 2018 *IEEE Trans. Appl. Supercond*. **28** 6800207
[24] Fujishiro H, Kaneyama M, Tateiwa T and Oka T 2005 *Jpn. J. Appl. Phys.* **44** L1221–L1224
[25] Fujishiro H, Hiyama T, Naito T, Tateiwa T and Yanagi Y 2008 *Material Science and Engineering B* **151** 95–100